Scaleable, microstructured plant for steam reforming of methane

E.L.C. Seris [a], G. Abramowitz [a], A.M. Johnston [b], B.S. Haynes [a],*

[a] *School of Chemical and Biomolecular Engineering, University of Sydney, NSW 2006, Sydney, Australia*
[b] *Optint, Edgecliff, NSW 2027, Sydney, Australia*

Abstract

We report results obtained in a demonstration plant for hydrogen production at $5\,Nm^3\,h^{-1}$ in a microchannel system constructed using techniques proven in Heatric printed-circuit heat exchangers (PCHE). The manufacturing technique allows great complexity in the design to be achieved with little incremental cost and our plant takes advantage of this to carry out the combustion and reforming reactions in highly integrated multiple adiabatic beds (MAB). The PCHE manufacturing technique is scaleable and the results from this small-scale plant demonstrate not only a practical miniplant for distributed manufacture of hydrogen but also provide the design basis for much larger plant (for example for transport fuelling and industrial applications) based on replication of the plate structures.

The system operated at 2 bar to produce hydrogen for a notional PEM fuel cell, with essentially complete conversion of natural gas in the reformer to equilibrium yields of CO, CO_2 and H_2 (~80%). The plant showed excellent turn-down characteristics to 30% of design capacity.
© 2007 Elsevier B.V. All rights reserved.

Keywords: Printed-circuit heat exchanger; Methane; Multiple adiabatic bed; Heat balances; Steam reforming

1. Introduction

Chemical plants are large, and getting larger, because economies of scale reduce the unit costs of production. Large plants are centralised because they can share site zoning and utilities such as power, steam, and cooling water. As a result, the size and concentration of chemical plants is always increasing, with globalisation and international trade working to penalise sub-"world scale" production. Isolated economies such as Australia's, and those of many developing countries, increasingly fail to be able to provide the capital or the market to be able to sustain world-scale production.

This paper describes work to create a new generation of chemical manufacturing systems that can be used in competitive small-scale and distributed production of commodity and specialty chemicals. We describe and demonstrate a technique for the creation of highly intensified, highly integrated chemical plants. The process is implemented using printed-circuit heat exchanger (PCHE) techniques in which the fluid passages and vessels are etched into flat plates, with the plates being stacked and bonded to create highly integrated modules. The manufacturing technique allows extraordinary complexity in the routing of fluid streams through the process, thus enabling very high levels of process integration to be achieved without significant capital or plant volume penalty [1–3]. The fine passages employed in the structure have characteristic dimensions around 1 mm, thus promoting further process intensification especially in heat transfer.

The PCHE technique produces scaleable modules ideally suited to a wide range of production capacities, from miniplant to world scale. The microstructured steam reforming plant studied here explores the concept of distributed manufacture based on miniplants, as espoused by Ponton and Benson [4] more than 10 years ago. We believe this paradigm offers new opportunities for chemical processing in smaller and more isolated economies such as in Australia and in developing countries. This will reduce the local dependence on imports and improve security of supply. For developing countries without the capital to invest in large plant, it offers a route for growth of their chemical industries at proportionate rates.

1.1. Distributed chemicals manufacture

The advantages of distributed chemical manufacture in smaller on-site or regional facilities were recognised by Benson and Ponton [4]. Not only would such plant be cheaper to build, it would offer improved safety (both in the process and in the bulk storage and transport of chemical products), and better reliability and continuity of supply. Today we can add the need

---

* Corresponding author. Tel.: +61 2 9351 3435; fax: +61 2 9351 3471.
E-mail address: b.haynes@usyd.edu.au (B.S. Haynes).

to reduce the risk of terrorist assault on critical infrastructure as a further driver for distributed manufacture.

A further advantage of a miniaturized chemical plant that can operate competitively at very small scales of production is that such plant is transportable by truck or by ship, for example, to process distributed or stranded resources.

Distributed production in relatively small, local facilities will enable producers to move from highly concentrated material sources (well- or pipe-head) to dispersed feedstocks of lower energy or carbon content such as biomass, facilitating the transition "from hydrocarbon to carbohydrate" feedstocks that underlies a long-term vision of sustainable production.

1.2. Microstructured systems

We have recently described an approach to the small-scale production of hydrogen by steam reforming of natural gas, conceived as part of a distributed power generation system based on 7 kW fuel cells [1]. This design satisfies Benson and Ponton's [4] two key approaches for the development of miniaturised plant and distributed manufacture, namely:

(1) Advanced manufacturing techniques are needed to produce the basic plant module in large numbers. The economies of scale inherent in using individual large plants are shifted to the replicate manufacture of many plants. Our reformer is constructed from plates into which fine (∼1 mm) fluid passages are cut; the plates are stacked and bonded to create process modules. Replicate manufacture of these microfluidic plates allows significant unit cost reductions as the number of systems increases. This manufacturing technology is proven in the commercial production of printed-circuit heat exchangers (PCHE) [5].

(2) New process designs are needed: miniplants cannot be developed simply by implementing existing processes on a minute scale. The printed-circuit manufacturing technique allows complex fluid circuitry to be readily implemented in microfluidic plates, without significant impact on the cost of manufacture. This creates opportunities for the implementation of novel process architecture. In particular, exceptionally high levels of process integration can be realized, allowing very high energy efficiency to be achieved without significant extra cost. The design thermal efficiency of our steam-methane reformer process [1] is >95% of the theoretically achievable value, which compares favourably with best-practice efficiencies achievable at large scale.

Microfluidic plate stack technology offers a practical route to "numbering up": each plate can have many parallel channels; many plates are bonded to form the basic core modules; and many modules can be combined to form the final unit. Different scales of operation can then be achieved by simply increasing the number of modules rather than through custom designs for each application – in the limit, one could go from bench-scale to industrial scale in a single step without risk. Scaling by "numbering up" the systems additionally allows capital investment

and market growth to be coupled, further reducing the financial risk of building large new facilities.

2. Process design

2.1. Multiple adiabatic beds

Catalytic plate reactors have received a great deal of attention in the literature, especially for the coupling of endothermic reaction demands with exothermic processes. An alternative approach, which we employ, is the use of multiple adiabatic beds (MAB), with heat interchangers between the beds. This is of course quite a traditional approach to temperature control in chemical reaction, but combined with PCHEs certain advantages arise:

- The beds are located in slots within a heat exchange block, thus avoiding interconnecting piping and the need to redistribute the reactants to each bed after heat exchange. In this way, many stages of adiabatic reaction and heat exchange can be employed, making the approach applicable to high heat load reactions such as reforming. A saw-tooth temperature pattern results, with the size of the teeth inversely proportional to the number of them, so that temperatures can be held between any required bounds (Fig. 1). Overall isothermal, ascending or descending temperature profiles can be created.
- The catalyst beds can be presented to the reactants with a short flow path and large face area, allowing the use of small catalyst particles with high effectiveness. Very compact reactors, with 'normal' pressure drops can be constructed.
- Conventional, proven catalyst forms can be employed in configurations which allow ready replacement of the catalyst in accessible, "large" slots. The only variation which might be preferred for the catalyst is smaller particle sizes than for tubular reactors to assist process intensification. Crushing of conventional sizes is a makeshift option. In many cases a preferred catalyst form would be coated ceramic monolith, in order to minimise pressure drop—this is the approach adopted in the present plant.
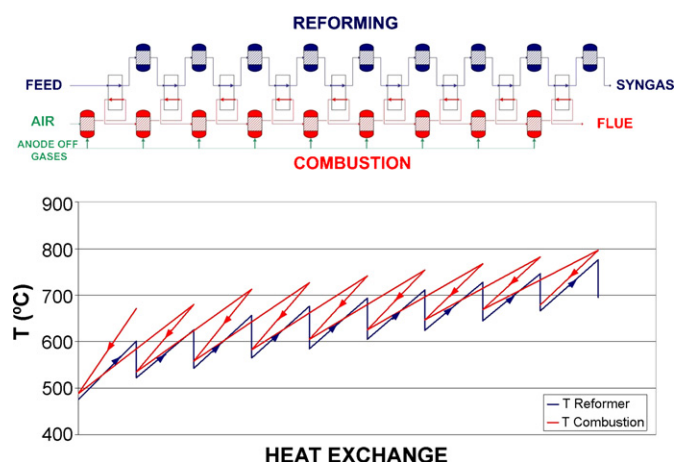

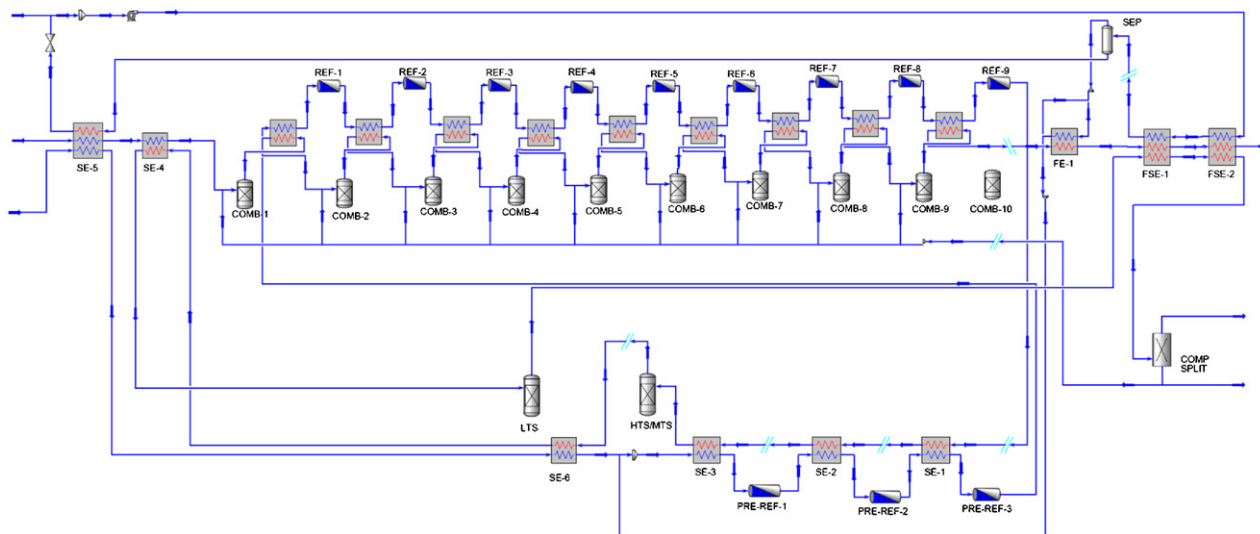Fig. 1. Saw-tooth pattern for the temperature profile in the reforming and combustion module.

Fig. 2. Process flow diagram for the micro-structured plant.

- The heat transfer area and catalyst volume in the reactor are decoupled. The ratio between the two volumes can be varied at will, depending on the heat loads and heat transfer fluid temperature.
- Periodic injection of fresh reactants is readily incorporated, thereby allowing the extent of exothermic reactions to be safely limited in each stage. For example, the process heat in the steam-methane reformer is supplied by the stagewise heat release that occurs when fresh fuel is fed into each stage [1,6]—the oxidant (air) fed into the first stage is progressively vitiated as it passes through successive stages and the overall mixture leaves the system as flue gas containing just a few percent of oxygen.

2.2. Process integration

The low cost of creating heat exchange elements and bringing process fluids to them in microchannel plate structures provides opportunities for high degrees of process integration. The SMR reformer achieves >95% of theoretical efficiency through the use of many stages of heat exchange in the process.

2.3. Process control

Numerous control elements are clearly not desirable in small-scale, distributed systems. We therefore employ passive (self-regulating) control wherever possible. Techniques include:

- Heat exchangers are sized and configured such that the overall reactor temperature profile (such as in Fig. 1) is maintained even under conditions of substantial turn-down.
- Counterflow and co-flow exchangers are employed. Both pinch up as flow rates fall, without substantially affecting boundary temperatures.
- The parallel splits in the fuel supply to the catalytic combustors are "hard-wired" into the assemblies, and require no active control.

2.4. Steam reforming process

The steam reformer process flow diagram in Fig. 2 shows the high degree of heat integration achieved using the PCHE and multiple adiabatic beds (MAB) technology. The plant can be divided into four sections (Fig. 3): the pre-reformer, the main block (including reforming, combustion and boiling), the steam drum and the low temperature water gas shift reactor (LTS).

The main plant module, contains 9 reforming reactors, 10 combustors and 11 heat exchangers in a single integrated block. The configuration of this module, incorporating MAB approaches for both the combustion and the reforming streams is described in detail elsewhere [1,3] and is the subject of a patent [1]. The combustion occurring in this block is the only heat input to the process, providing heat not only for the endothermic reaction but for steam generation too.
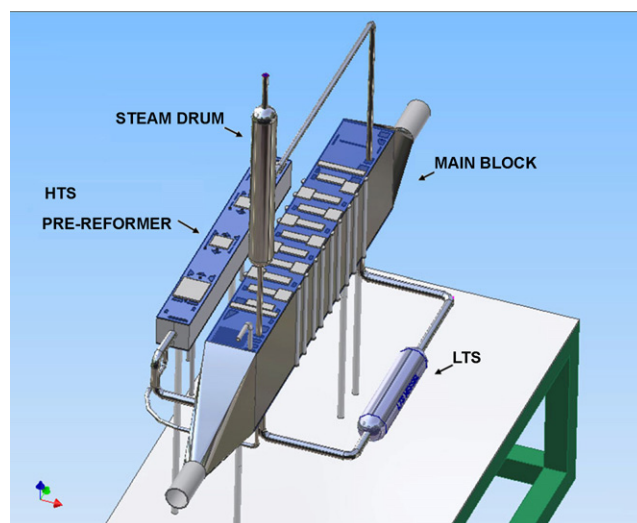

Fig. 3. 3D representation of the steam reforming pilot plant. The length of the main block is about 700 mm.

Table 1
Composition of desulfurised natural gas (mole fraction)

CH_4	0.908
CO_2	0.021
N_2	0.019
C_2H_6	0.052
Total	1.000

The reforming reaction was carried out at an absolute pressure of approximately 2 bar since the plant was conceived as a fuel processor for a PEM fuel cell that would operate at slightly above atmospheric pressure. The reformer catalyst was a proprietary monolith-supported, noble metal catalyst (Engelhard). The combustion side operated at atmospheric pressure and employed a proprietary palladium-based, monolith-supported catalyst (Engelhard).

3. Pilot plant

The reformer has been tested in a stand-alone pilot scale plant [3], producing hydrogen at a rate of $5\,Nm^3\,h^{-1}$. The composition of the desulfurised natural gas used as the reformer feedstock is given in Table 1. Comprehensive measurements of temperatures, pressures and compositions have been taken throughout the process, including after every stage of reaction. Fig. 4 shows the system prior to wrapping with insulation and closure of the surrounding box—the complex piping for the diagnostic measurements would not be present in a commercial installation.

3.1. Pressure drop

The pressure drops through the system were measured. Here, we report only the overall values in order to emphasis that microchannel plate systems need not operate with excessive pressure drops. The pressure drop in the air flow through the combustion side of the reforming system was <5 kPa for an inlet air pressure of 120 kPa—in our tests, the combustion side had to
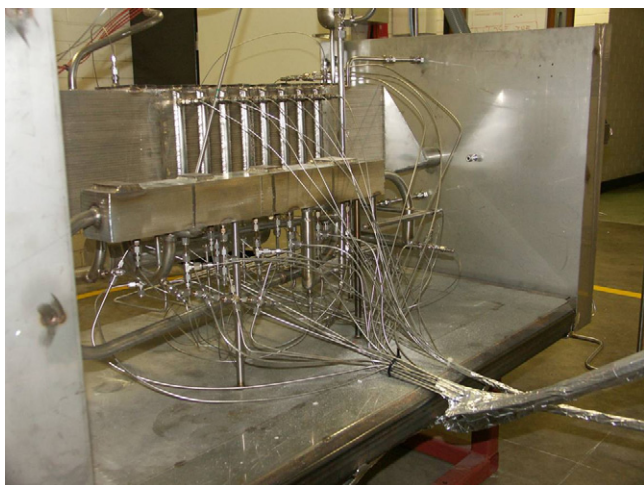

Fig. 4. Reformer with piping for sampling, pressure taps and thermocouples. The surrounding box was filled with insulation and sealed before testing.

be backpressured slightly to achieve adequate flow through the sampling system whereas in practice this would not be required so this side would operate very close to atmospheric pressure.

On the reformer side, the inlet natural gas pressure was 235 kPa and there was a 70 kPa pressure drop through the system.

3.2. Material balances

The reaction stoichiometry in the reformer is expressed in terms of three independent equations:

$$C_2H_6 + H_2 \rightarrow 2CH_4 \tag{R1}$$

$$CH_4 + H_2O \rightarrow CO + 3H_2 \tag{R2}$$

$$CH_4 + 2H_2O \rightarrow CO_2 + 4H_2 \tag{R3}$$

Note that the water gas shift reaction does not appear here since it is a combination of Eqs. (2) and (3). Product measurements, on a dry basis, were made of all the species in the above reactions as well as of N_2. The dry mole balance table, referred to an inlet CH_4 amount of 1 mol is given in Table 2:

Because the measurements are made on a dry basis, we cannot directly invoke a hydrogen or oxygen material balance in evaluating the measurements in terms of mole balance table (Table 2). However, there remain three independent equations to be used to check the consistency of the measurements: the normalisation equation (sum of mole fractions = 1), the nitrogen balance and the carbon balance.

Fig. 5 shows the measured species mole fraction sum for the products of each reactor on the reforming side of the process. Overall, the raw composition measurements show an accurate mole fraction sum that is close to the expected value of unity. However, there are clear trends in going from the early stages, where the sum is about 105%, to the later stages (~100%), suggesting some small systematic errors in the measurements of the reactants (predominantly CH_4) versus the products (H_2, CO and CO_2).

Natural gas was the only source of nitrogen to the reforming section. Therefore, nitrogen can be used as an internal reference since its molar flow remains constant throughout the whole section. We can thus write,

$$\frac{n_{CO}}{n_{N_2}} = \frac{x_{CO}}{x_{N_2}} = \frac{a}{\gamma} \tag{1}$$

Table 2
Mole balance table for reactions (R1)–(R3)

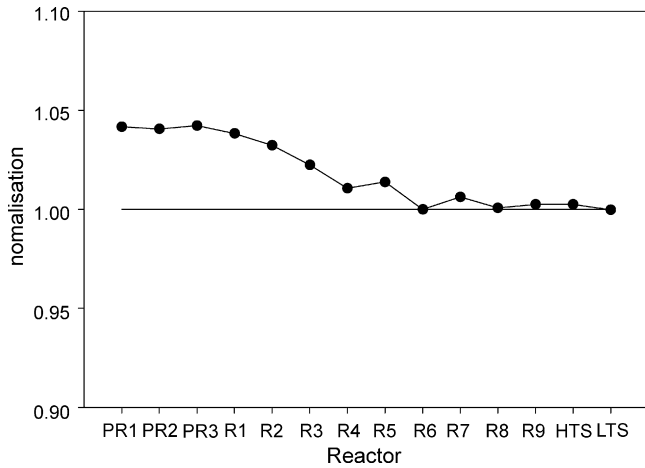| Species	Moles in	Moles out
CH_4	1	$1 + 2(\alpha + c) + \beta - a - b$
C_2H_6	α	c
CO_2	β	b
N_2	γ	γ
CO	0	a
H_2	0	$3a + 4(b - \beta) - \alpha + c$
Total	$1 + \alpha + \beta + \gamma$	$1 + \alpha - 3\beta + \gamma + 3a + 4b$

Fig. 5. Mole fraction sum of measured products on a dry basis for the reaction products after each stage of reaction. PR; refers to a pre-reforming stage; R: denotes a reforming stage; and HTS and LTS are the high- and low-temperature sift stages, respectively.

Hence,

$$a = \frac{x_{CO}}{x_{N_2}} \times \gamma \tag{2}$$

Similarly, we can write:

$$b = \frac{x_{CO_2}}{x_{N_2}} \times \gamma \tag{3}$$

$$c = \frac{x_{C_2H_6}}{x_{N_2}} \times \gamma \tag{4}$$

We define the ratio R_N^0 as the number of moles of nitrogen coming out of a given reactor over the initial number of moles of nitrogen introduced into the reformer section:

$$R_N^0(i) = \frac{n_{N_2} \text{ leaving reaction stage } i}{n_{N_2} \text{ entering the system}} = \frac{n_{TOT} \times x_{N_2}(i)}{n_{TOT_0} \times x_{N_{2_0}}} \tag{5}$$

Taking expressions for n_{TOT}, a and b from Table 2 and Eqs. (2) and (3) yields:

$$R_N^0(i) = \frac{1 + \alpha - 3\beta + \gamma}{\gamma} \times x_{N_2}(i) + 3x_{CO}(i) + 4x_{CO_2}(i) \tag{6}$$

Note that R_N^0 represents the combined effects from entry to stage i. An error in the entry composition is propagated through every stage. Therefore, we can similarly define the stagewise mole balance ratio R_N to represent the nitrogen balance across the i-th reactor:

$$R_N(i) = \frac{R_N^0(i)}{R_N^0(i-1)} \tag{7}$$

The experimental ratios $R_N(i)$ are plotted in Fig. 6 where it seen that the nitrogen balance across any individual stage is closed within 4%. Note that, because the overall mass balance is assumed in determining n_{TOT}, these ratios do not reveal any material loss but they do provide a direct assessment of measurement quality.
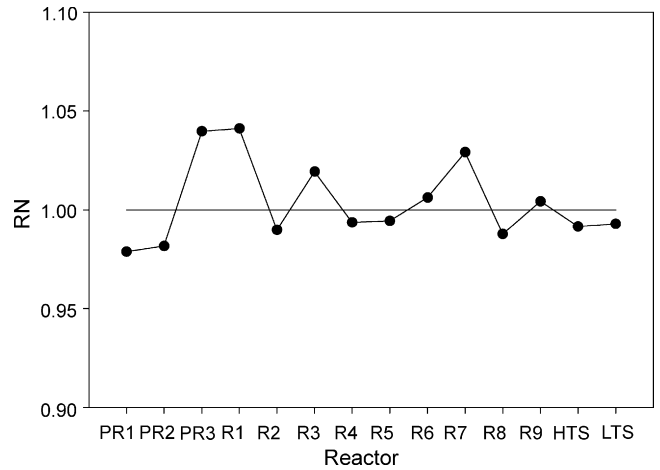

Fig. 6. Nitrogen balances across each reactor.

The experimental carbon mass balance can be assessed along similar lines using R_C^0 and R_C:

$$R_C^0(i) = \frac{n_C \text{ leaving reaction stage } i}{n_C \text{ entering the system}}$$

$$= \frac{n_{TOT} \times (x_{CH_4}(i) + x_{CO}(i) + x_{CO_2}(i) + 2x_{C_2H_6}(i))}{n_{TOT_0} \times (x_{CH_{4_0}} + x_{CO_0} + x_{CO_{2_0}} + 2x_{C_2H_{6_0}})}$$

$$= \frac{x_{CH_4}(i) + x_{CO}(i) + x_{CO_2}(i) + 2x_{C_2H_6}(i)}{((1 + 2\alpha + \beta)/\gamma) \times x_{N_2}(i)} \tag{8}$$

The carbon balance across a reaction stage i is then calculated as

$$R_C(i) = \frac{R_C^0(i)}{R_C^0(i-1)} \tag{9}$$

The experimental ratios $R_C(i)$ are plotted in Fig. 7 which reveals that the carbon balance is noisier than was found for the nitrogen balance, with fluctuations around the expected value of up to 13%.
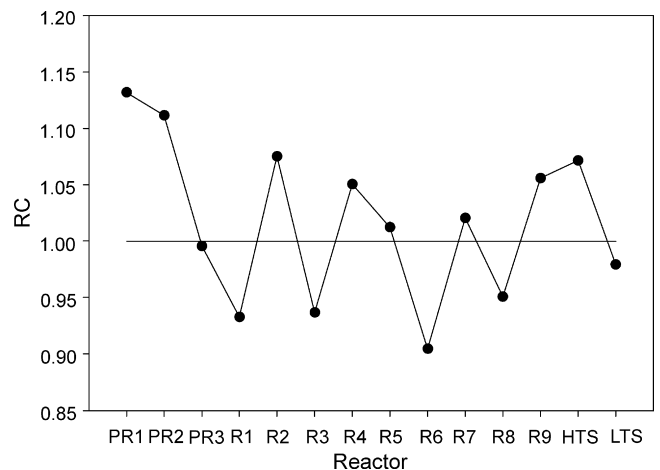

Fig. 7. Carbon balances across each reactor.

3.3. Data reconciliation

We have employed data reconciliation to adjust the experimental data to match the constraints provided by the mole fraction sum and the nitrogen and carbon balances – i.e. to force the results in Figs. 5–7 to equal the expected value of unity in every case. Satisfaction of the constraints leads to adjusted data that are more accurate than the measured data [7].

We seek to solve the following optimisation problem:

$$\begin{cases} \mathbf{A}\hat{\mathbf{x}} = \mathbf{c} \\ \underset{\hat{\mathbf{x}}}{\text{Min}}(\mathbf{y} - \hat{\mathbf{x}})^{\mathrm{T}}\mathbf{W}(\mathbf{y} - \hat{\mathbf{x}}) \end{cases} \tag{10}$$

where $\mathbf{A}$ is the constraint matrix, $\mathbf{c}$ a constant vector, $\mathbf{W}$ the weight matrix (which represents the random errors), $\mathbf{y}$ the measurement vector and $\hat{\mathbf{x}}$ the solution vector. For a linear problem such as the present one, the vector solution $\hat{\mathbf{x}}$ is found analytically using the method of Lagrange multipliers.

$$\hat{\mathbf{x}} = \mathbf{y} - \mathbf{W}^{-1}\mathbf{A}^{\mathrm{T}}(\mathbf{A}\mathbf{W}^{-1}\mathbf{A}^{\mathrm{T}})^{-1}(\mathbf{A}\mathbf{y} - \mathbf{c}) \tag{11}$$

The measurement vector $\mathbf{y}$ is of dimension 6. Its components are the compositions of the following species: H_2, CO, CO_2, CH_4, N_2 and C_2H_6. Three constraints were available using the normalisation equation, the carbon balance and the nitrogen balance. The weight matrix is a diagonal matrix, taken to be the inverse of the measurement variance for the individual species—these variances were obtained from the standard deviations of repeated measurements of the sample composition at the steady-state operating condition presented in Table 3.

Figs. 8 and 9 show the raw and reconciled data for H_2 and CO_2, respectively. The species compositions that are adjusted most to meet the data reconciliation constraints are the CO_2 and N_2 compositions. Overall, the measurement adjustments are greatest in the early stages where the raw measured concentration sum was about 105%.

4. Discussion

4.1. Heat balances

The overall heat balance between process input streams and process output streams closed within 2.2% of the total system heat transfer duty. Individually, the pre-reformer block and the main block presented, respectively, an imbalance of 0.5% and 2.7% of their total duties. The heat distribution in the integrated reformer block agreed closely with design calculations incor-

Table 3
Relative standard deviation for repeated steady-state composition measurements

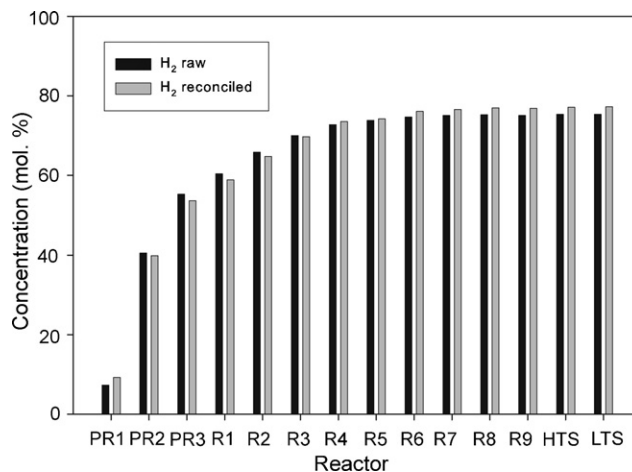| Species	Relative standard deviation (%)
H_2	7.88
CO_2	2.66
CO	2.14
CH_4	1.60
C_2H_6	1.27
N_2	3.80

Fig. 8. Comparison of measured and reconciled H_2 compositions.

porating heat transfer by convection, conduction and radiation. The overall thermal efficiency of the process (defined as reformer product lower heating value over the sum of the reforming and combustion feed lower heating values) was within 5% of the predicted value for the test conditions [1].

4.2. Approach to equilibrium

Fig. 10 shows the compositions of the reformer gas stream through the conversion process in three stages of pre-reforming and nine stages of reforming. The design temperature profile increases steadily through the conversion process but temperatures were not experimentally accessible within the integrated block structure. Reliable temperatures were obtained only for the gases leaving each of the pre-reformer stages and for the final exit temperature, as shown by the open symbols in Fig. 10.

Equilibrium temperatures were calculated from the reconciled composition data, assuming equilibration of reaction (R2) (SMR) and the water gas shift reaction (WGS) at the measured pressure at each location. As can be seen in Fig. 10, the water gas shift reaction is clearly equilibrated early, with $T_{\text{WGS}} = T_{\text{expt'l}}$ already in the second pre-reformer stage. The steam-methane
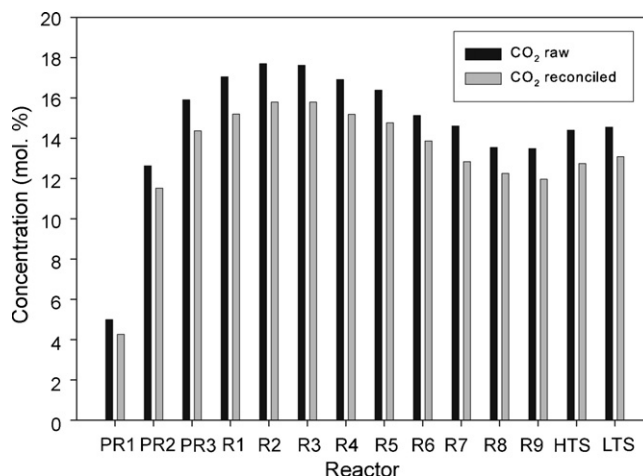

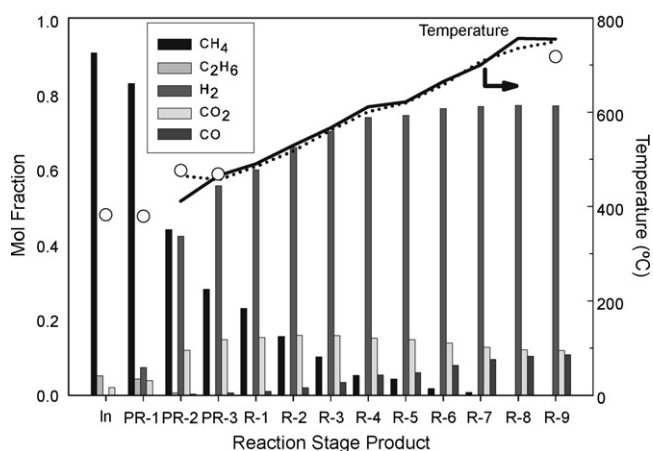Fig. 9. Comparison of measured and reconciled CO_2 compositions.

Fig. 10. Results for steam-methane reformer demonstration plant at 100% capacity. Bars show dry reconciled composition of gases leaving individual stages. Open points show measured temperatures and lines show calculated equilibrium temperatures based on measured compositions for reforming (solid line) and water–gas shift (dashed line).

reforming reaction is equilibrated in the products of the third pre-reformer stage, $T_{SMR} = T_{expt'l}$. The close agreement between T_{WGS} and T_{SMR} in the remaining reforming stages suggests that both of these reactions are equilibrated in those stages. The equilibration of the WGS reaction is expected from the fast kinetics of this process, but the results for the SMR reaction suggest that the individual stage reactors may be oversized for this duty—i.e. that the system could support a significantly higher throughput than designed for, or that the beds could be sized down if necessary.

It is common practice for catalyst manufacturers simply to specify an amount of catalyst needed for a specific feed composition and flow rate, based on a maximum space velocity for the conversion. The present results make it clear that this global specification is not sufficient for the design of our highly integrated set of reactors: it is important to know the extent of reaction that will occur in each differential reaction stage. We are currently obtaining much more detailed characterization of various catalysts for use in design and optimisation of multiple adiabatic bed systems.

4.3. Compactness

The compactness of the plant is evaluated by considering the ratio of the hydrogen production flow rate over the reactor volume. This ratio is compared in Table 4 with a traditional steam reformer [8] and the catalytic wall reactor (CWR) described by Tonkovich et al. [9]. This shows that the MAB process achieves a compactness at least comparable with CWR systems. In fact, the comparison in Table 4 is weighted against the MAB system which is a fully integrated plant, including steam raising and water gas shift reactors whereas the other units are for the reforming process only.

As discussed above, the present plant operated very close to equilibrium throughout and was therefore oversized to some extent. Moreover, the present system operates at low pressure (2 bar) since its nominal application is as a fuel processor for an atmospheric pressure PEM fuel cell. Enhanced compactness

Table 4
Comparison of process intensity for different reformer reactors

Reactor type	Hydrogen production flow rate over reactor volume ($m^3\,s^{-1}\,m^{-3}_{reactor}$)
Traditional steam reformer [8]	0.011
14 bar catalytic wall reactor [9]	0.113
2 bar demonstration plant (MAB technology)	0.085
15 bar MAB steam reformer	0.134

Note that the fully integrated MAB systems include steam raising and shift reactors whereas the data for the other rector types refer only to the reforming reactor.

of the MAB will be obtained by operating at higher pressures such as would be required to drive a membrane or pressure-swing adsorption system for hydrogen purification or for syngas generation for further processing in GTL or ammonia synthesis. A 14-bar system is currently being tested in our laboratories – as shown in Table 4, it is designed for an integrated process intensity for hydrogen production about 50% higher than the present 2-bar system.

5. Conclusions

We have demonstrated the performance of a fully integrated steam-methane reformer plant incorporating multiple adiabatic beds and intense heat integration. The entire system, which comprises 23 reactors and 18 heat exchangers, is implemented in two microchannel plate modules plus a steam drum and low-temperature shift reactor to produce hydrogen for a notional PEM fuel cell. The microchannel modules are fabricated via the replicate method developed by Heatric for its commercially proven and widely used printed-circuit heat exchangers (PCHE).

The plant produced a stream containing 80% hydrogen at a rate of $5\,Nm^3\,h^{-1}$. The process intensity is approximately one order of magnitude greater than is achievable in conventional large-scale reformers and there are no efficiency penalties in achieving this because of the very intensive process integration. The intense process integration and other design features ensured a high degree of autoregulation. The PCHE construction technique means that the system is scaleable and provides the basis for hydrogen production over a wide range of applications and market sizes. Testing of a higher-pressure unit, operating at 14 bar, is currently underway.

Acknowledgements

References

[1] A.M. Johnston, B.S. Haynes. Heatric Steam Reforming Technology, AIChE (2002), Spring National Meeting, in: C.-W. Chiu, R.D. Srivastava, R. Mallinson (Eds.), Proceedings of Conference on Natural Gas Utiliza-

tion, AIChE, New Orleans; pp. 380–385, 2002. (See also International Patent Application PCT/AU03/00022, International Publication No.WO 03/055585 A1.).

[2] http://v3.espacenet.com/textdoc?DB=EPODOC&IDX=WO03055585&QPN=WO03055585. Currently in national phase, patents pending.

[3] E.L.C. Seris, G. Abramowitz, A.M. Johnston, B.S. Haynes, Demonstration plant for distributed production of hydrogen from steam reforming of methane, Chem. Eng. Res. Design 83 (2005) 619–625.

[4] R.S. Benson, J.W. Ponton, Process miniaturization—a route to total environmental acceptability, Chem. Eng. Res. Design 71 (1993) 160–168.

[5] http://www.heatric.com.

[6] G. Abramowitz, B.S. Haynes, Microreaction Process Heating, in: Proceedings of the 19th International Symposium on Chemical Reaction Engineering, Potsdam, Germany, 2006.

[7] S. Narasimhan, C. Jordache, Data Reconciliation and Gross Error Detection: and intelligent use of process data, Gulf Publishing Company, 2002.

[8] M. Zanfir, A. Gavriilidis, Catalytic combustion assisted methane steam reforming in a catalytic plate reactor, Chem. Eng. Sci. 58 (2003) 3947–3960.

[9] A.Y. Tonkovich, S. Perry, Y. Wang, D. Qiu, T. LaPlante, W.A. Rogers, Microchannel process technology for compact methane steam reforming, Chem. Eng. Sci. 59 (2004) 4819–4824.